SAND2007-0693J

Simultaneous Mapping of Temperature and Stress in Microdevices Using Micro-Raman Spectroscopy

Thomas Beechem and Samuel Graham

Woodruff School of Mechanical Engineering
Georgia Institute of Technology
Atlanta, GA 30332-0405

Sean P. Kearney, Leslie M. Phinney, and Justin R. Serrano

Engineering Sciences Center
Sandia National Laboratories,
Albuquerque, NM 87185-0834

Abstract

Analysis of the Raman Stokes peak position and its shift has been frequently used to estimate either temperature or stress in microelectronics and MEMS devices. However if both fields are evolving simultaneously, the Stokes shift represents a convolution of these effects, making it difficult to measure either quantity accurately. By using the relative independence of the Stokes linewidth to applied stress, it is possible to deconvolve the signal into an estimation of both temperature and stress. Using this property, a method is presented whereby the temperature and stress were simultaneously measured in doped polysilicon microheaters. A data collection and analysis method was developed to reduce the uncertainty in the measured stresses resulting in an accuracy of ±40 MPa for an average applied stresses of -325 MPa and temperature of 520°C. Measurement results were compared to 3-D finite-element analysis of the microheaters and were shown to be in excellent agreement. This analysis shows that Raman spectroscopy has the potential to measure both evolving temperature and stress fields in devices using a single optical measurement.

I. Introduction

The reliability of many microscale devices depends on the presence of induced temperature or stress fields which may lead to hard or soft failures during operation. While much modeling and metrology has focused on the measurement of such fields, many times it is their coupled thermomechanical behavior which is of most concern to the device scientist or engineer. Examples of such coupled behavior arise in the packaging of devices where coefficient of thermal expansion mismatch can cause failure in fragile electronic die or interconnect structures upon thermal loading. Other examples where thermomechanical effects become important is in the reliability of polar semiconductors like GaN RF-devices, high brightness LEDs, and multilayer thermal MEMS (e.g., thermal actuators, heaters, and micro-power sources). Due to the microscale critical dimensions in such devices, the direct and detailed measurement of these coupled temperature and stress fields have remained a challenge, but are important for verifying device performance and validating models.

In order to determine coupled thermal and mechanical effects in devices, often temperature measurements are first performed and then used in either analytical or finite-element codes to predict the resultant stress state. For microscale devices, temperature measurement techniques include micro-infrared imaging, scanning thermoreflectance, liquid-crystal thermometry, as well as micro-Raman spectroscopy [1-5]. In general, optical techniques are preferred as they are often less invasive and non-destructive. An excellent review of such techniques has been provided by Zhang [6].

While such routines exist for measuring temperature fields in a variety of devices, obtaining stress fields with similar spatial resolution is quite challenging. Most stress

measurement procedures center on the direct measurement of deformation or strain which is subsequently transformed into stress. Measuring deformation can be accomplished using a variety of techniques such as profilometry, optical interferometry, or X-ray diffraction [7,8]. Using the measured deformation field, either finite-element analysis or analytical approaches must then be incorporated to calculate the level of stress in the device. In either case, knowledge of the mechanical properties of the material is imperative to the estimation of stress.

One notable exception arises in Raman spectroscopy which does not rely on this direct measurement of deformation in order to determine stress. Rather, probing the anharmonic characteristics of a Raman-active crystal lattice under strain provide a direct estimation of stress. This technique has been applied to a number of materials and devices including single crystal silicon, diamond, SiC, GaN, MEMS, and CMOS circuit elements [9-13]. In addition, this technique is one of a select few that is sensitive to both temperature and stress fields providing a unique capability for probing combined thermomechanical responses in materials.

Measurement of either temperature or stress using Raman spectroscopy most often centers on measurement of the change in the Stokes-shifted peak position. This change is then transformed to actual temperature or stress values using an appropriate calibration standard. Under combined thermomechanical loading, this change in peak location becomes convoluted due to the simultaneous effects of both temperature and stress relegating the accurate measurement of either parameter difficult. In spite of this fact, simultaneous measurement of both temperature and stress using Raman spectroscopy is possible, through use of an additional characteristic of the spectrum, namely the linewidth

of the Stokes-shifted peak [14-16]. The Raman linewidth, Γ, is stress insensitive to the first order and can be used as a measurement of temperature even in the presence of a mechanical loading. By monitoring both the shift in the Stokes peak location as well as its linewidth, the deconvolution of stress and temperature in Raman-active materials and devices can be achieved. Such a metrology tool will be invaluable for measurements during device operation providing insight into both performance and reliability.

In this work, we explore the concept of using the dual features of the Raman spectrum of silicon to measure the stress and temperature distribution in doped polysilicon microheaters. First, we will review some of the relevant fundamental background on the effects of temperature and stress on the Raman response. Then we will present our experimental procedure and data analysis method which is used to reduce noise and uncertainty in the measured values. Finally, a comparison with 3-D finite-element simulations is made in order to validate the efficacy of the metrology method.

II. Theory

A. The Raman Effect

The shift in photon energy which occurs with Raman scattering can be understood by considering the interaction of photons with a vibrating crystal lattice. In general, two properties can be defined by the electronic distribution within a crystal lattice in equilibrium, namely, the dipole moment, P, and electric polarizability, α. These properties will change with deviation in equilibrium interatomic spacing of the lattice or time-dependent vibrational motions around these equilibrium positions. The electric polarizability is a second order tensor response function which represents the volume and

shape of the charge distribution in the lattice. When a photon with electric field, E, is incident on the lattice, the induced dipole moment is given by,

$$P = \varepsilon_o \alpha \mathrm{E} \tag{1}$$

where εo is the free-space permittivity. Since phonons are present in the crystal lattice, we must consider changes in the electric polarizability tensor which can be described through a Taylor series expansion about the equilibrium position of the lattice atoms

$$\alpha = \alpha_o + \frac{d\alpha}{dq} q + ... \tag{2}$$

where α_o is the polarizability at the equilibrium lattice spacing and $q = q_o \cos(\omega_o t)$ is the time-dependent change in the lattice spacing due to phonon vibrations with amplitude q_o and frequency ω_o. Realizing that the incoming electric field, $E = E_o \cos(\omega t)$, can be written as an oscillatory function of amplitude E_o and frequency ω, using Equation (2), we may now write Equation (1) in its expanded form

$$P = \varepsilon_o \alpha_o E_{\ o} \cos(\omega t) + \frac{d\alpha}{dq} \varepsilon_o q_o \cos(\omega_o t) E_o \cos(\omega t) \tag{3}$$

where ω_o is the frequency of the phonon vibration and ω is the vibrational frequency of the incident photon. Applying a trigonometric identity to (3) leads to the following relation,

$$P = \varepsilon_o \alpha_o E_{\ o} \cos(\omega t) + \frac{d\alpha}{dq} \frac{\varepsilon_o q_o E_o}{2} \cos\left((\omega_o - \omega)t\ \right) + \frac{d\alpha}{dq} \frac{\varepsilon_o q_o E_o}{2} \cos\left((\omega_o + \omega)t\right) \tag{4}$$

The first term on the right hand side of Equation (4) accounts for Rayleigh scattering of photons. The second and third terms result in Stokes and anti-Stokes Raman scattering, respectively, where the photons are shifted away from their incident frequency ω by an

amount equal to the optical phonon frequency ω_o [17]. Thus stress and temperature dependence of the Raman response enters through the effect of the phonon vibrations in the crystal lattice on the scattered light signal.

B. Temperature Dependence of the Raman Signal

When considering the Raman scattering of photons using visible monochromatic laser light, the conservation of energy and momentum generally require that photons interact with optically coupled phonons near the Brillouin zone center, such that ω_o in (4) corresponds to the zone-center optical phonon [18]. Thus, the temperature dependence of the phonons in the vicinity of zone center will help explain the temperature dependence of the Raman response. In general, the phonon vibrational modes and their dispersion can be modeled by considering a spring-oscillator system if the force laws between the atoms or molecules in the lattice are known. The solution for this type of classical oscillator reveals that the resulting lattice vibrational frequencies vary with the interatomic forces [19]. As the lattice is heated or cooled, the equilibrium positions of the atoms are displaced, resulting in an overall volumetric expansion or contraction of the lattice and a change in interatomic forces [20]. These changes in the interatomic forces modify the phonon vibrational frequencies which are reflected in the Raman phonon spectra.

In addition to this volumetric contribution, interactions between the phonons themselves augment the frequency shift as well [20]. This occurs as changes in the lattice vibrational energy alter the interatomic potentials between the atoms. The lattice vibrational energy in turn is governed by the Bose-Einstein distribution of thermal

occupation resulting in a purely temperature dependent shift in the phonon frequency. This portion of the frequency shift is often referred to as the explicit contribution.

The temperature dependence of the linewidth arises solely from this phonon population distribution around the zone center. According to the Heisenberg uncertainty principle, the energy of a phonon can only be measured within a certain specificity if there is only a finite measurement time. This is described mathematically according to the energy-time uncertainty relation:

$$\Gamma \approx \Delta E = \frac{\hbar}{\tau} \tag{5}$$

where Γ is the width of the Raman line, $\hbar = 5.3 \times 10^{-12}$ cm^{-1}s, and τ is the scattering time for a phonon [21]. From Equation (5) it is seen that the measured linewidth of a Raman peak will vary with scattering time of the optically coupled phonon mode. This scattering time will be dependent both upon type and frequency of a phonon as well as the presence of other phonons. Consequently, linewidth is sensitive to the phonon population near the zone center as well. Thus, the Stokes peak shift depends both on the volume-induced changes in the phonon frequency as well as thermal phonon population near the zone center, while the linewidth is entirely determined by the thermal contribution.

C. Stress Dependence of the Raman Signal

To illustrate the effect of stress and deformation on the Raman signal, consider two objects connected by a spring of force constant K. The relative displacement of one mass, u, can be described using the dynamic relation shown below where $\bar{m}$ is the reduced mass of both objects and $\ddot{u}$ is the acceleration of that mass.

$$\bar{m}\ddot{u} = Ku \tag{6}$$

If this spring were harmonic, the frequency of the normal modes could easily be found to be equivalent to $\omega = \sqrt{K/\bar{m}}$. In reality, however, the spring constants connecting two atoms are in fact anharmonic and hence vary with strain. This variance can be described using Equation (7) where ε is the applied strain:

$$\frac{\partial K}{\partial \varepsilon}\varepsilon = K^1\varepsilon \tag{7}$$

To account for the effect of this anharmonicity, Equation (6) must be modified as follows:

$$\bar{m}\ddot{u} = \left(K + K^1\varepsilon\right)u \tag{8}$$

To find the frequency change of the normal mode vibrations with strain this equation must be solved. Using material-dependent phonon deformation potentials (PDP), the modified spring constant can be described as $K^1 = \bar{m} \times f(p,q,r)$ where p,q, and r are the PDP. Ganesan et. al. derived the solution for silicon using the following secular equation [22].

$$\begin{vmatrix} p\varepsilon_{11} + q\left(\varepsilon_{22}+\varepsilon_{33}\right) - \lambda & 2r\varepsilon_{12} & 2r\varepsilon_{13} \\ 2r\varepsilon_{12} & p\varepsilon_{22} + q\left(\varepsilon_{11}+\varepsilon_{33}\right) - \lambda & 2r\varepsilon_{23} \\ 2r\varepsilon_{13} & 2r\varepsilon_{23} & p\varepsilon_{33} + q\left(\varepsilon_{11}+\varepsilon_{22}\right) - \lambda \end{vmatrix} = 0 \tag{9}$$

In the above relation, ε_{ij} are the strain tensor components and λ_j are the eigenvalues for phonon polarization modes j. The difference in frequencies of Raman spectra with (ω_j) and without strain ($\omega_{o,j}$) can be correlated using these eigenvalues according to the relation:

$$\lambda_j = \omega_j^2 - \omega_{o,j}^2 \tag{10}$$

In the special case of biaxial strain common in many MEMS and microelectronic thin film devices, $\varepsilon_{12} = \varepsilon_{23}=\varepsilon_{13}=0$, and the secular equation reduces to:

$$\begin{vmatrix} p\varepsilon_{11}+q(\varepsilon_{22}+\varepsilon_{33})-\lambda & 0 & 0 \\ 0 & p\varepsilon_{22}+q(\varepsilon_{11}+\varepsilon_{33})-\lambda & 0 \\ 0 & 0 & p\varepsilon_{33}+q(\varepsilon_{11}+\varepsilon_{22})-\lambda \end{vmatrix}=0 \quad (11)$$

For Raman backscattering from the (001) surface of Si, this solution results in the following relationship between frequency shift and stress [9]:

$$\Delta\omega = -3.85\left(\frac{\sigma_{xx}+\sigma_{yy}}{2}\right) \quad (12)$$

where $\Delta\omega$ is the frequency shift in cm^{-1} and the linear shift coefficient is -3.85 cm^{-1}/GPa. This equation shows that the stress-induced frequency change is dependent only upon an elastic deformation of the crystal lattice. This occurs as the application of stress changes the equilibrium position of the atoms in the lattice and hence the phonon vibrational frequencies. Thus, a similar dependence of the Stoke peak shift response is seen as in the case of a temperature change.

However, the impact of stress on the phonon population distribution is very weak and can be neglected as long as the phonon density of states remains relatively static. This is a valid assumption as long as measurements take place at relatively moderate temperatures and pressures [20]. With these assumptions of the stress-independent phonon population distribution, the linewidth should not change in the presence of an evolving stress field. Therefore a temperature measurement determined from the measured linewidth is independent of stress and can be used to deconvolve the combined impact of stress and temperature on the Raman peak position. In this manner, Raman spectra can be utilized for simultaneous measurement of temperature and stress.

D. Determination of Stress and Temperature

For many Raman active materials near room temperature and above, the Stokes-shifted peak position shows a linear dependence with respect to temperature in the absence of stress [15]. Temperature can be calculated by monitoring the shift in the Stokes peak based on Equation (13):

$$\omega = A\left(T_\omega - T_o\right) + \omega_o \tag{13}$$

where ω is the measured Stokes-shifted peak position of a particular mode, T_ω is the "peak-based" temperature, A is a calibration constant, and ω_o is the Stokes-shifted peak position at room temperature, T_o. The measured value of ω is biased by the impact of stress in the material. The magnitude of this stress-induced bias is given by,

$$\omega = D\sigma + \omega_o \tag{14}$$

where D is the calibrated stress constant and σ is the average stress.

An unbiased measure of the temperature can be obtained from the parabolic relationship between the linewidth and temperature as approximated in Equation (15)

$$\Gamma = B\left(T_\Gamma - T_0\right)^2 + C\left(T_\Gamma - T_0\right) + \Gamma_o \tag{15}$$

where $T_\Gamma = T$ is the unbiased "linewidth-based" temperature, B and C are calibration constants, and Γ_o is the linewidth at room temperature. It should be noted that the value of Γ_o is dependent both upon material crystalline quality as well as instrument broadening effects strongly affected by the slit width of the spectrometer.

The combined stress and temperature effect on the Stokes peak location can then be determined by combining Eqs. (13) and (14).

$$\omega = A\left(T_\omega - T_o\right) + D\sigma + \omega_o \tag{16}$$

To deconvolve the temperature and stress effects seen in the Stokes peak response (Equation (16)), the linewidth can be used to provide a temperature measurement that is unbiased by the applied stress T_Γ. If there is no change in stress in the device, the Stokes peak-based temperature, T_ω, should result in the same value as the linewidth-based temperature, T_Γ, given by Equation (15). A discrepancy in temperature between the two methods is an indication of stress evolution in the device as was stipulated by Abel et. al [15]. To calculate the stress, this discrepancy in temperature is transformed to an equivalent change in the Stokes frequency shift which is subsequently used to calculate the applied stress from Equation (14). A simplification of these steps is given in Equation (17) which provides a compact form for calculating the applied stress in the device:

$$\sigma = \frac{\left(T_\omega - T_\Gamma\right) A}{D} \tag{17}$$

Based on this relation, the presence of a tensile stress will result in an over prediction of the Stokes-peak-based temperature ($T_\omega > T_\Gamma$), while compressive stresses will induce an under prediction by the Stokes-peak-location method ($T_\omega < T_\Gamma$).

III. Experimental

A. Sample Preparation

To investigate the thermal stress evolution in a MEMS structure during operation, polysilicon microheaters were analyzed using a micro-Raman mapping procedure. The device consisted of a phosphorous doped polysilicon beam deposited on a 3.9 μm thick layer of thermal oxide which rested on a 500 μm thick layer of silicon. The microheater

was 10 μm wide by 300 μm long and had a thickness of 2.2 μm. The final doping of the microheater was 10^{20} atoms/cm^3 and was achieved using an ion implantation procedure. Details of the fabrication scheme can be found elsewhere [23]. A schematic of the structure is shown in figure 1. The devices were used without releasing them from the underlying oxide layer in order to constrain the deformation of the beam creating appreciable levels of thermal stress.

B. Raman Measurement System

A Renishaw InVia Raman Microscope with 180º backscattering geometry was used for all measurements in this study. With a spectrometer focal length of 250 mm and a diffraction grating of 3000 lines/mm, a spectral dispersion of 0.46 cm^{-1}/pixel was obtained with a slit width of 50 μm. A slit width of 50 μm provides sufficient detection capabilities with maximum signal levels at the expense of some spectral resolution. However, this resolution is sufficient for detecting Stokes peak shifts within ±0.057 to 0.1 cm^{-1} from Voigt fits of the isolated Si Raman line. Samples were measured using a 488-nm Ar^+ laser set to an incident power sufficiently low to ensure there was no Stokes peak shift due to laser heating. A 50X objective with a numerical aperture (NA) of 0.5 was used to focus the probe laser beam and collect the Raman signature of the samples.

The temperature response of the Stokes peak and linewidth were measured for a monolithic single-crystal silicon sample, which was mounted in an unconstrained manner in a temperature controlled hot stage (Linkham TS 1500). This yielded a stress-free sample which was used to compare the peak position and linewidth measurement techniques in order to provide the inherent uncertainty in the stress determination. Raman spectra were acquired in 100°C increments from room temperature to 500°C as

described elsewhere [14,16]. Twenty five spectra were taken at each temperature with acquisition times adjusted to obtain a Stokes peak with at least 6000 CCD counts. The average values of the Stokes peak position and linewidth at each temperature, determined from Voigt curve fitting of the spectra, were then used to calibrate the Raman response versus temperature. The peak position and linewidth show a linear and parabolic fit, respectively, as described by Eqs (13) and (15) and shown in figures 2 and 3 (See Table 1 for calibration constants). In each case, the correlation constant was greater than 0.99.

It should be noted that the calibration of linewidth as a function of temperature depends on the microstructure of the material; a smaller linewidth is observed with improved crystalline quality which results from longer phonon lifetimes as per Equation (5). However, the relative change in linewidth ($\Gamma - \Gamma_o$) is much less dependent on microstructural effects. The change in linewidth with temperature arises due to phonon-phonon scattering mechanisms, whose rate is primarily determined by temperature dependent population of phonons available for scattering. While defects in the microstructure can increase phonon-boundary scattering and broaden the Raman linewidth, the defect's contribution to temperature dependent changes is small as compared to phonon-phonon scattering. This is true as long as the microstructure remains stable with increasing temperature. This effect is seen in figure 4 where the relative change in Raman linewidth ($\Gamma - \Gamma_o$) is plotted for several polysilicon and single-crystal silicon samples. When the offset, Γ_o, is subtracted all of the data collapse to a single curve, which suggests that the calibration of single-crystal Si can be applied to the samples in our study. By using single crystalline Si, we ensure that the calibration of

temperature dependent Raman characteristics come from a stress-free sample for our analysis.

A calibration was also performed to determine the Raman response under an applied stress using single crystalline Si. Using a four point bending stage, the response of silicon to various levels of stress was analyzed both in compression and tension as described elsewhere [14,16]. The Stokes peak position was found to vary linearly with stress (D = -3.6 cm^{-1}/GPa, Equation (14)) at a rate within 10% of the predicted biaxial constant given by De Wolf as given in Equation (12) [9]. The linewidth, however, showed no detectable dependence on the state of stress as seen in figure 3.

With knowledge regarding the temperature and mechanical response of silicon, full temperature and stress fields were obtained on the polysilicon microheater through incorporation of a mapping procedure. The mapping procedure was carried out using an automated x-y stage with 0.5 micron resolution. Raman spectra were sampled at 2 μm intervals across the beam width and 6 μm periods along the length. Acquisition times were once again varied to Stokes peaks with intensities of at least 6000 CCD counts on the microheater for each level of power dissipation. Thermal stress evolution was probed by first taking a map of the beam at room temperature to account for residual stress in the beam. With the residual stress known, the temperature and stress evolution could then be analyzed through maps taken at heater powers of 240 and 480mW.

IV. Results and Discussion

A. Temperature measurements

Figure 5 displays the 2D linewidth temperature maps of the microheater as a function of heater input power. The temperatures were observed to be fairly uniform throughout

the microheater at each power level. Only near the ends of the microheater, where the interconnect pads serve as a thermal sink, is there an appreciable temperature gradient. Since the stress distribution should follow the temperature distribution, this mapping procedure indicates that the stress should be relatively constant in the middle of the heater as well. Such simple physical profiles provide a known response against which the measured values of stress and temperature can be compared, and from which the precision in the measurements can be estimated from the scatter in experimental data.

A comparison between the Stokes peak shift and linewidth based temperature profiles of the powered microheater are shown in figure 6. The results show a significant difference between the two measurements, being on the order of 30°C at 240 mW and 60°C at 480 mW of dissipated power. Considering the fact that the uncertainty in stress measurements using Raman has been reported to be ±25 MPa [24], this would correspond to a temperature difference between the two methods of ±4.1°C. As shown in figure 6, the discrepancy between temperature measurements is much greater than this threshold, indicating that significant stress is present in the device, as expected. Furthermore, since the predicted peak position based temperature is less than the linewidth-based value a compressive stress is anticipated. The next sections will then enumerate how to quantify this stress in a manner that minimizes uncertainty.

B. Uncertainty in the Calculation of Stress

The uncertainty in the stress measurement is predominately controlled by the uncertainty in measuring the Stokes linewidth. To estimate the inherent uncertainty in our system, stress-free single-crystal Si was inserted into a Linkham environmental test stage and heated to temperatures between 100 - 500°C. By measuring the Stokes shifted

peak position and the change in linewidth, the calibration constants from Table 1 were used to determine the sample temperatures using Eqs. (13) and (15). A total of 25 Raman spectra were taken at each temperature in order to average the peak position and linewidth. Differences in the measured temperatures were then used to calculate the stress in the sample using Equation (17), knowing that the induced stress should be zero. This resulted in a typical variation in the stress measurements on the order of +/- 40 MPa as shown in figure 7. Additional acquisitions were not seen to significantly reduce this variance and hence the magnitude will be used as the intrinsic scatter in the measurement for the rest of this study.

C. Determination of Stress from Mapping Procedure

Moderate levels of noise in the measurement of the linewidth-based temperature, T_Γ, can introduce significant noise in the measured stress profiles. To mitigate this effect, we fit the T_Γ results to an expected functional form of the temperature profile. The unreleased beam structure was modeled by considering an energy balance between 1D axial conduction, uniform Joule heating, and lateral heat losses which were proportional to the surface area and local temperature. With constant thermal conductivity and electrical resistivity, the governing differential equation for this steady state heat transfer problem is given by

$$\frac{d^2\theta}{dx^2} - M\theta + Q = 0 \qquad (18)$$

where x is the axial position along the heater, and $\theta = \theta(x) - T_{ref}$ is the difference between the local heater temperature and an appropriate reference temperature, M is a parameter describing the relative importance of lateral heat losses to axial conduction,

and Q represents the relative importance of Joule heating to axial conduction. The solution to Equation (18) is given by

$$\theta(x) = \frac{Q}{M^2} + K_1 \sinh(Mx) + K_2 \cosh(Mx) \tag{19}$$

where K_1 and K_2 are constants.

By using Equations (13) and (15) to compute T_ω and T_Γ and fitting the form of Equation (19) to the T_Γ data set, Equation (17) was used to estimate the stress throughout the microheater. In addition, a simultaneous and stress-bias-free measure of the device temperature profile is given by the T_Γ data set as shown in figure 6. While the specific functional form shown in Equation (19) works well for MEMS with 1D conduction, it may also be possible to use other generalized functions such as polynomials, Fourier series, etc., to fit data sets for arbitrary geometries. The use of generalized functions, however, requires additional assessment to determine the appropriate order of the function to be used in order to ensure there is no reproduction of high frequency scatter in the data. The need for this type of filtering function can be reduced with a reduction of the uncertainty in T_Γ.

D. Comparison of mapping results to finite-element analysis

To verify the calculation of stress obtained from the Raman mapping procedure, a finite-element model was developed using ANSYS 9.0 with multi-physics elements. Temperature dependent values for the thermal conductivity and thermal expansion coefficient were employed, while other material properties were assumed constant for each of the three materials: polysilicon, silicon dioxide, and silicon [25].

The model itself incorporated a fine mesh in the polysilicon beam and silicon dioxide layers to accurately resolve the temperature and stress distribution. The linewidth-based

temperature measurements, smoothed using Equation (19), were used as the surface boundary condition of the beam in the thermal analysis [23]. An additional boundary condition was obtained by placing a thermocouple on the backside of the silicon substrate during operation of the microheater. Mechanical boundary conditions were assumed to be fixed in the vertical direction on the bottom of the substrate while two orthogonal edges were fixed leaving the opposite edges free to expand within the plane.

Figure 8 shows a comparison of the stress calculated from the Raman measurements and the finite-element analysis for a microheater power of 240 mW and 480 mW. The data show fairly good agreement with the stress averaged over the heater of σ_{FEA} = -160 MPa and σ_{Raman} = -153 MPa. A similar trend was also seen at a power dissipation level of 480 mW with maximum stress levels of σ_{FEA} = -348 MPa and σ_{Raman} = -304 MPa. Although scatter can be seen in the acquired Raman data, variations are largely within the inherent uncertainty of the system at the lower power dissipation level. The difference between the measurement and FEA analysis grows to 44 MPa at the higher power dissipation level. It believed that this is due to the use of a temperature independent Young's modulus in the finite-element calculation. With a microheater temperature of 520°C, a reduction in the modulus of the polysilicon is expected resulting in a reduction of stress in the device, a fact not captured by the model. However, both data sets show encouraging results suggesting that it is possible to perform a stress analysis on devices under thermal loading using Raman spectroscopy.

V. Conclusions

Micro-Raman spectroscopy was used to simultaneously obtain complete temperature and biaxial stress maps of a functioning polysilicon microheater. Comparison of the

measurements to 3D finite-element calculations suggests that the method holds promise for applications in active devices where thermomechanical processes are of importance. While linewidth-based temperature measurements are typically not as precise as Stokes-shifted peak position thermometry, the use of analytical smoothing functions allows for more accurate results. It should also be noted that we have analyzed a biaxial state of stress which is a limitation for applying 180° backscattered Raman experiments on silicon. This is due to the optical phonon degeneracy in Si. However more detailed information of the stress state may be possible in materials which do not show such degeneracy at the zone center. Overall, the method provides one of the only experimental techniques which can nondestructively measure stress and temperature in devices. Techniques such as this may find wide ranging applications in power generating MEMS and wide-band-gap semiconductors, where high temperatures are expected and the presence of stress can change device performance or reliability.

Acknowledgements

Support for this research was provided by the NSF CAREER Award CTS- 0448795 and Sandia National Laboratories under the Laboratory Directed Research and Development (LDRD) and Microsystems and Engineering Sciences Applications (MESA) programs. Sandia is a multiprogram laboratory operated by Sandia Corporation, a Lockheed-Martin Company, for the United States Department of Energy's National Nuclear Security Administration under Contract DE-AC04-94AL85000.

References

[1] D. G. Cahill, W. K. Ford, K. E. Goodson, G. D. Mahan, A. Majumdar, H. J. Maris, R. Merlin, and S. R. Phillpot, Journal of Applied Physics **93,** 793-818 (2003).

[2] J. Park, M. W. Shin, and C. C. Lee, IEEE Electron Device Letters **24** (2004).

[3] J. Pomeroy, M. Kuball, D. Wallis, A. Keir, P. Hilton, R. Balmer, M. Uren, and T. Martin, Applied Physics Letters **87,** 103508 (2005).

[4] R. J. Stoner and H. J. Maris, Physical Review B **48,** 16373-16387 (1993).

[5] P. W. Webb, Circuits, Devices and Systems, IEE Proceedings G **138,** 390 (1991).

[6] Z. M. Zhang, in *Annual Review of Heat Transfer*; *Vol. 11*, edited by C.-L. Tien (Begell House, Inc., New York, 2000), p. 351-411.

[7] B. Bhushan, *Springer Handbook of Nanotechnology* (2004).

[8] M. Pruessner, T. King, D. Kelly, R. Grover, L. Calhoun, and R. Ghodssi, Sensors and Actuators A: Physical **105,** 190-200 (2003).

[9] I. De Wolf, Semiconductor Science and Technology**,** 139 (1996).

[10] J. Kim, J. F. JR., P. Klein, S. Jang, F. Ren, and S. Pearton, Electrochemical and Solid State Letters **8,** G45-G47 (2005).

[11] L. A. Starman, J. A. Lott, M. S. Amer, W. D. Cowan, and J. D. Busbee, Sensors and Actuators A: Physical **104,** 107-116 (2003).

[12] W. Zhu, J. Zhu, S. Nishino, and G. Pezzotti, Applied Surface Science **252,** 2346-2354 (2006).

[13] J. C. Zingarelli, M. A. Marciniak, and J. R. Foley, in *Detection of residual stress in silicon carbide MEMS by Micro-Raman spectroscopy*, San Francisco, CA, USA, 2005 (Materials Research Society), p. 1392.

[14] M. Abel, Thesis, Georgia Institute of Technology, 2005.

[15] M. Abel, S. Graham, J. Serrano, S. Kearney, and L. Phinney Journal of Heat Transfer, in press., Journal of Heat Transfer**,** In Press (2006).

[16] M. Abel, T. Wright, E. Sunden, S. Graham, W. King, and M. L. Lance, in *Thermal Metrology of Silicon Microstructures using Raman Spectroscopy*, 2005, p. 235-242.

[17] D. A. Long, *Raman Spectroscopy* (McGraw-Hill, 1977).

[18] M. Balkanski, R. F. Wallis, and E. Haro, Physical Review B **28,** 1928 (1983).

[19] C. Kittel, *Introduction to Solid State Physics*, 8th ed. (Wiley, Hoboken, NJ, 2005).

[20] G. Lucazeau, Journal of Raman Spectroscopy **34,** 478-496 (2003).

[21] B. Di Bartolo, *Optical Interactions in Solids* (John Wiley & Sons, New York, 1968).

[22] S. Ganesan, A. Maradudin, and J. Oitmaa, Annals of Physics **56,** 556-594 (1970).

[23] M. Abel and S. Graham, in *Thermometry of Polycrystalline Silicon Structures Using Raman Spectroscopy*, 2005, p. 1-8.

[24] V. Srikar, A. Swan, M. S. Unlu, B. Goldberg, and S. Spearing, Journal of Microelectromechanical Systems **12,** 779-787 (2003).

[25] P. U. T. P. R. Center, *Thermophysical properties of matter* (IFI/Plenum, New York, 1970-).

Table 1. Calibration Constants Calculating Biaxial Stress and Temperature

Equation (13)	$A = -0.022\ cm^{-1}/K$	
Equation (15)	$B = 6.7x\ 10^{-6}\ cm^{-1}/K^2$	$C = 4.14x10^{-3}\ cm^{-1}/K$
Equation (14)	$D = -3.6\ cm^{-1}/GPa$	

Figure Captions

Figure 1. Schematic of polysilicon doped microheater measuring 300 μm long by 10μm wide.

Figure 2. Stokes-shifted peak position under the effects of both temperature (top) and stress (bottom). The dual linear dependence of the Stokes-shifted peak position makes the measurement of either parameter impossible when both effects are present.

Figure 3. Stokes linewidth under the effects of both temperature (top) and stress (bottom). The linewidth varies parabolically with temperature while showing no correlation with respect to mechanical loading thus allowing for accurate temperature measurement even in the presence of stress.

Figure 4. Relationship between temperature and relative linewidth for single crystalline and several polycrystalline silicon samples. Data show that the temperature versus relative linewidth change is very similar regardless of the microstructural aspects of the silicon sample. The relative linewidth is defined as Γ-Γ_o from Equation (15).

Figure 5. Temperature (°C) maps of the beam at 240 mW (top) and 480 mW (bottom).

Figure 6. Temperature distribution across the length of the microheater when dissipating 240 mW (top) and 480 mW of power (bottom). The peak based method significantly under predicts the temperature indicating, as expected, that the beam is under a compressive stress.

Figure 7. The inherent variation in the stress measurements was determined to be +/- 40 MPa for the temperature range of interest in this study. The variation is primarily controlled by the scatter from the Stokes linewidth measurement.

Figure 8. Data comparison of biaxial stress calculated using finite-element analysis (FEA) and Raman spectroscopy for power dissipation levels of 240 mW (top) and 480 mW (bottom). At the higher power level, the Raman data shows a lower stress level than that calculated by FEA which is close to the inherent uncertainty of the system (±40 Mpa). This may be due to the use of a temperature independent modulus in the analysis.

Figure 1

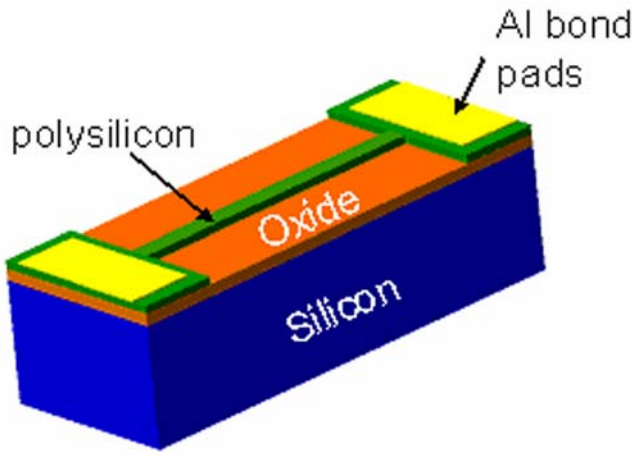

Figure 2

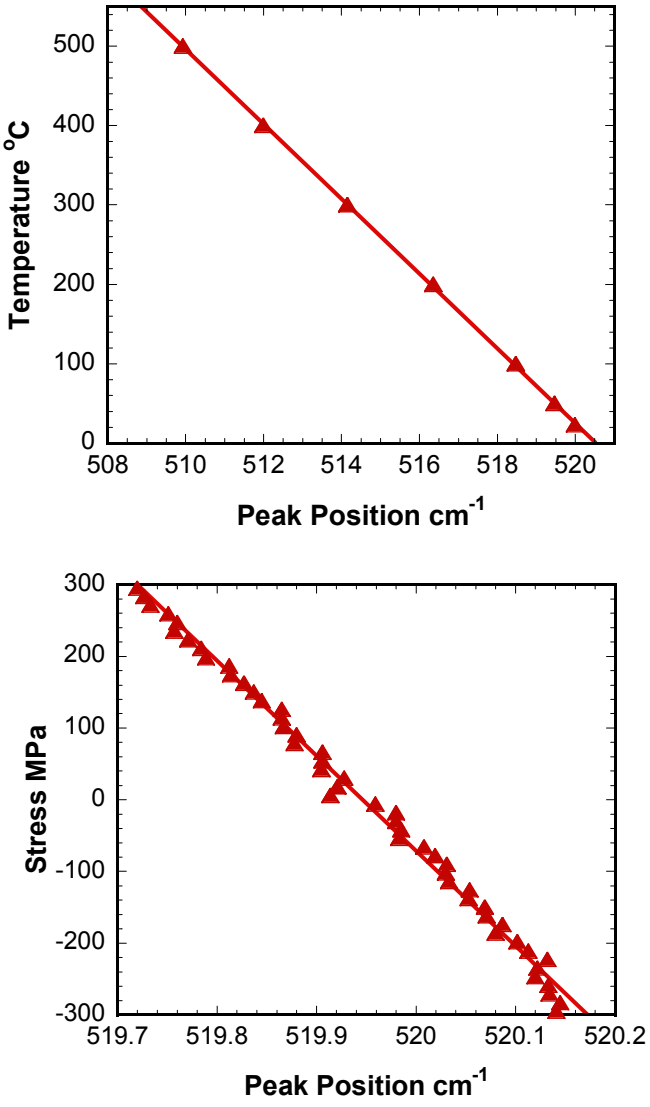
Temperature °C
500
400
300
200
100
0
508
510
512
514
516
518
520
Peak Position cm-1
Stress MPa
300
200
100
0
-100
-200
-300
519.7
519.8
519.9
520
520.1
520.2
Peak Position cm-1

Figure 3

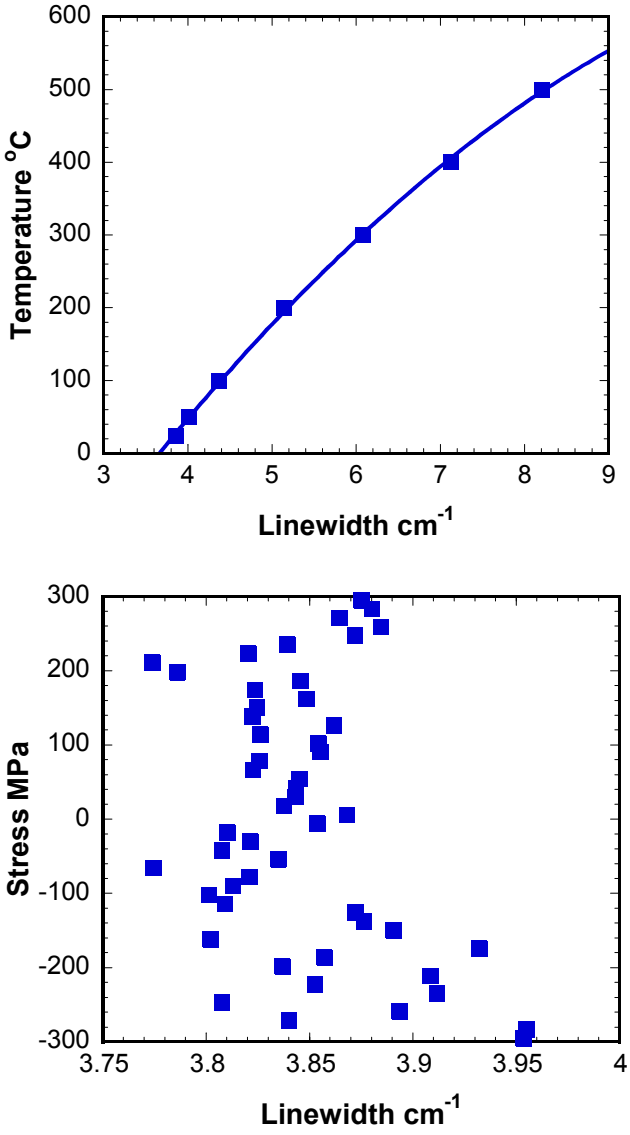
600
500
400
300
200
100
0
Temperature °C
3
4
5
6
7
8
9
Linewidth cm-1
300
200
100
0
-100
-200
-300
Stress MPa
3.75
3.8
3.85
3.9
3.95
4
Linewidth cm-1

Figure 4

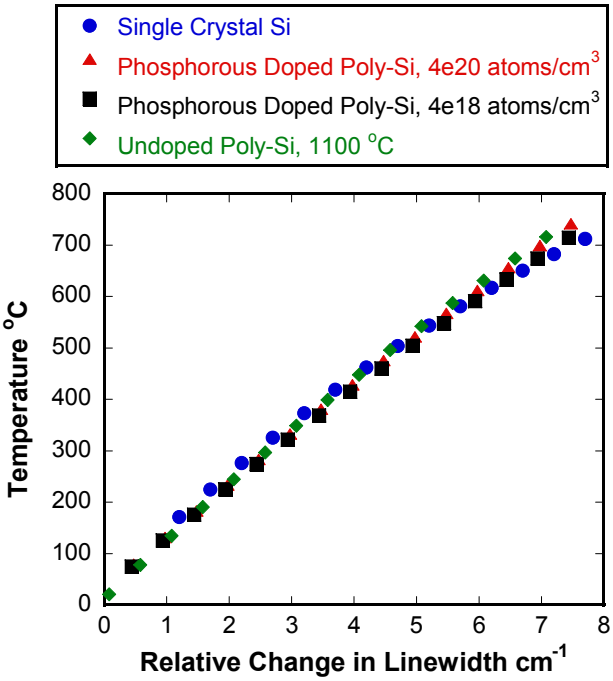
Single Crystal Si
Phosphorous Doped Poly-Si, 4e20 atoms/cm3
Phosphorous Doped Poly-Si, 4e18 atoms/cm3
Undoped Poly-Si, 1100 °C
Temperature °C
Relative Change in Linewidth cm-1
0
100
200
300
400
500
600
700
800
0
1
2
3
4
5
6
7
8

Figure 5

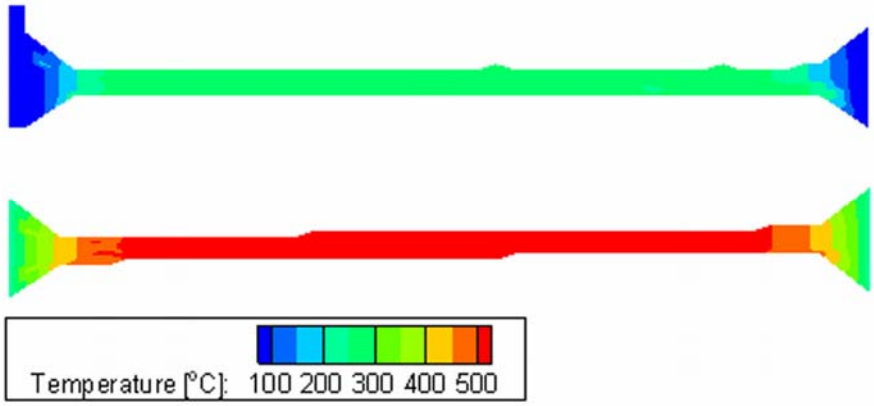

Figure 6

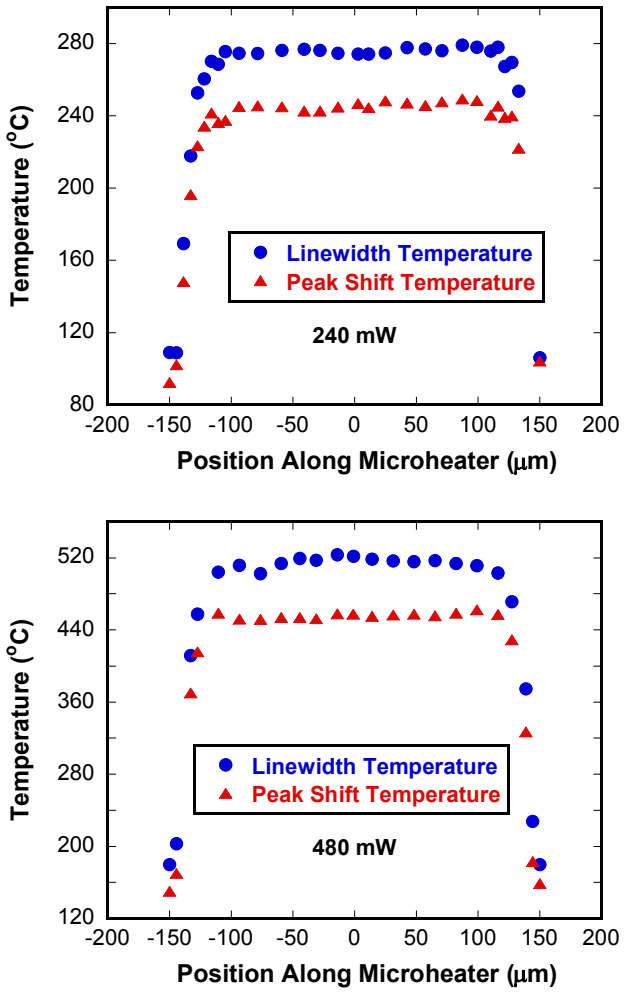
Temperature (°C)
280
240
200
160
120
80
-200
-150
-100
-50
0
50
100
150
200
Position Along Microheater (μm)
Linewidth Temperature
Peak Shift Temperature
240 mW
Temperature (°C)
520
440
360
280
200
120
Position Along Microheater (μm)
Linewidth Temperature
Peak Shift Temperature
480 mW

Figure 7

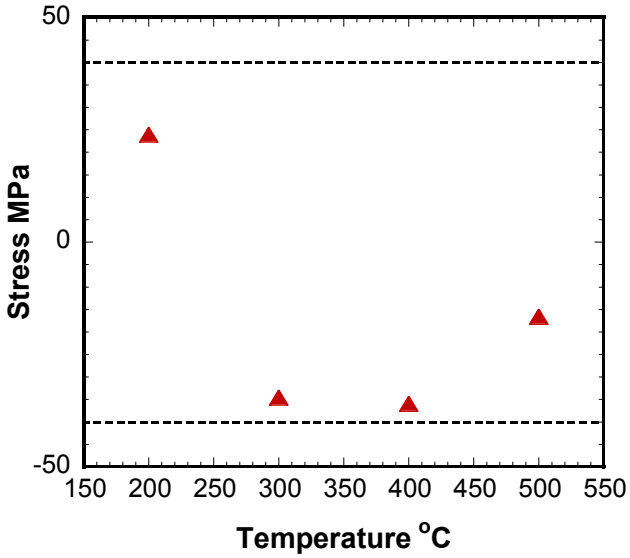
50
0
-50
Stress MPa
150
200
250
300
350
400
450
500
550
Temperature °C

Figure 8

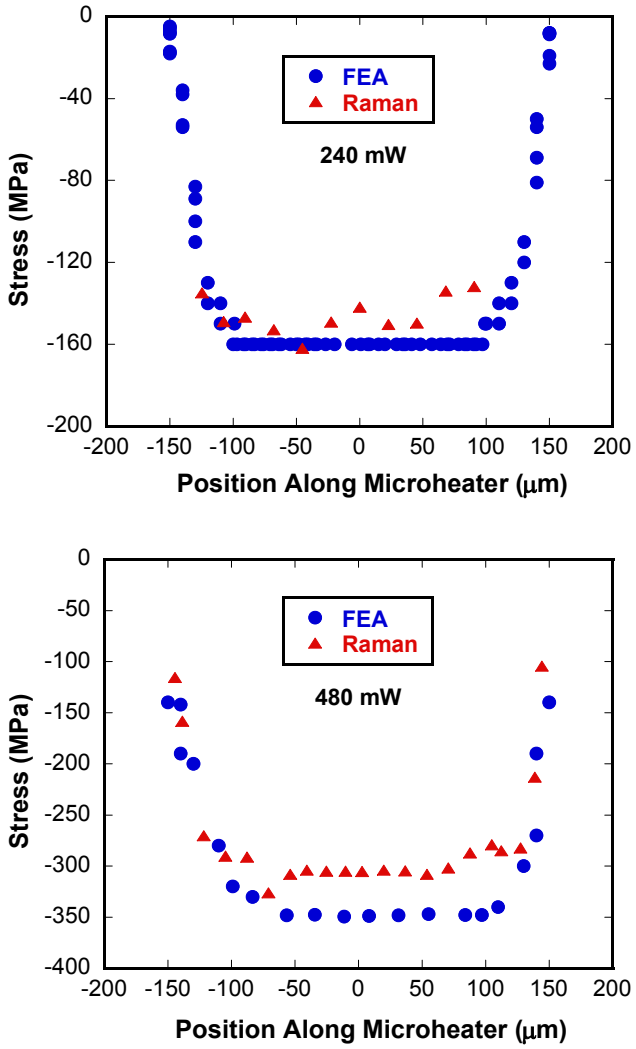
FEA
Raman
240 mW
Stress (MPa)
0
-40
-80
-120
-160
-200
-200 -150 -100 -50 0 50 100 150 200
Position Along Microheater (μm)
FEA
Raman
480 mW
Stress (MPa)
0
-50
-100
-150
-200
-250
-300
-350
-400
-200 -150 -100 -50 0 50 100 150 200
Position Along Microheater (μm)